Crystal Structure and Stability of Ammonium Azide Under High Pressure

Guozhao Zhang, Haiwa Zhang, Sandra Ninet, Hongyang Zhu, Cailong Liu, Jean-Paul Itié, Chunxiao Gao, Frédéric Datchi

Crystal Structure and Stability of Ammonium Azide under High Pressure

Guozhao Zhang[1,2] , Haiwa Zhang[2], Sandra Ninet[2], Hongyang Zhu[3], Cailong Liu[4], Jean-Paul Itié[5], Chunxiao Gao[1,], and Frédéric Datchi[2,*]*

[1]State Key Laboratory of Superhard Materials, Jilin University, Changchun 130012, China. [2]Institut de Minéralogie, de Physique des Matériaux et de Cosmochimie (IMPMC), Sorbonne Université, CNRS UMR 7590, MNHN, 4 Place Jussieu, F-75005 Paris, France.

[3]School of Physics and Electronic Engineering, Linyi University, Linyi 276005, China

[4]Shandong Key Laboratory of Optical Communication Science and Technology, School of Physical Science and Information Technology of Liaocheng University, Liaocheng 252059, China

[5]Synchrotron Soleil, L'Orme des Merisiers, Saint-Aubin, BP 48, 91192 Gif-sur-Yvette Cedex, France.

*Corresponding Authors

E-mail: cc060109@qq.com; frederic.datchi@sorbonne-universite.fr

ABSTRACT

Due to its potential applications as a high-energy density material, the high-pressure polymorphs of ammonium azide (AA) have received much attention recently. However, the crystal structure of phase II (AA-II), stable above 3.0 GPa, has remained elusive until now. By combining X-ray diffraction and Raman experiments with first principle calculations, we determine that AA-II is a hydrogen(H)-bonded structure of ammonium and azide ions with monoclinic symmetry, space group *P2/c*. The latter is comprised of alternating molecular layers of ammonium and azide ions and mostly differs from AA-I by its denser packing of molecular planes while preserving the hydrogen bond network. First-principle calculations show that phase II has the lowest enthalpy among all other considered structures from 4.9 to 102.6 GPa, pushing the phase transitions to the previously predicted hydro-nitrogen solids to higher pressures. Raman data to 85.0 GPa at room temperature confirm the absence of phase transition and agree very well with the pressure evolution of the Raman modes of AA-II predicted by our calculations.

I. INTRODUCTION

Searching polynitrogen materials which are (meta)stable at ambient conditions has been a subject of intense efforts in the recent past due to the potential applications of these materials as high energy density materials (HEDM)[1-4]. The N_2 molecular crystal transforms into the extended single-bonded cubic gauche phase of nitrogen (cg-N) above 110 GPa and 2000 K[5]. Unfortunately, cg-N is not recoverable at ambient conditions since it reverts to molecular N_2 below 40 GPa at 300 K[5]. Various groups have looked for potential new compounds that incorporate elements that could enhance the stability of nitrogen oligomers[6-10]. Among the latter, hydronitrogen (N_xH_y) compounds have been given particular attention, considering that their high mass ratio of nitrogen makes them

particularly attractive for HEDM and that hydrogen could effectively passivate polymeric structures at ambient conditions[1, 3, 8, 10]. Among many hydronitrogen compounds, ammonium azide (NH_4N_3) has been considered as a good potential precursor to poly-hydronitrogen. Indeed, the double bond of the azide ion N_3^- is weaker than the triple bond of N_2, and thus easier to break, which may provide a pathway to polymeric nitrogen at more tractable pressures.

Various works have investigated the possibility that AA converts to hydro-nitrogen solids (HNS) under high pressure[11-14]. At ambient pressure, AA adopts a distorted CsCl-type orthorhombic structure with the space group *Pmna*[15-17], noted AA-I or AA-*Pmna* hereafter. As illustrated in Figure 1(a), there are two crystallographic types of azide anions in this structure: type-I azide anions are perpendicular to the c-axis while type-II azide anions are rotated by an angle θ of 27.63° with respect to the c-axis. The predicted candidate structures for AA at high pressure[11-14, 18] may be grouped in three classes: 1) ammonium azide structures, consisting of ammonium cations and azide anions as in AA-I; 2) trans-tetrazene (TTZ) phases, consisting of H2N-N=N-NH2 molecules and 3) HNS solids. These structures are illustrated and labeled in Figure 1(a). Using theoretical calculations, Refs.[11-13] predicted that AA-*Pmna* first transforms to TTZ and then to HNS-1 with increasing pressure, with some differences in transition pressures (respectively, 36GPa and 75GPa for Ref.[11], 41.9GPa and 89.4GPa for Ref.[12], 39.3GPa and 79.8GPa for Ref.[13]). Liu and Zhang proposed that HNS-2 is stable between 5.6 and 15 GPa where it reverts to AA-*Pmna*[14]. Finally, Yu *et al*. suggested that another AA phase of structure *P2/c* is more stable that *Pmna* above 1.5 GPa and up to its transformation to the TTZ phase at 77 GPa[18].

Experimental studies of NH_4N_3 by high-pressure Raman and x-ray diffraction (XRD) experiments have established that there is a phase transition from AA-*Pmna* to a phase named AA-II at a pressure around 3.0 GPa [16, 19-20]. To date, the crystal structure of AA-II has remained elusive,

and no experimental evidence of other phase transition was found up to 71.2 GPa [12]. In order to address the potential application of NH_4N_3 in searching or synthesizing HEDMs, it is necessary to understand its crystal structure and physical properties under high pressure, which makes the determination of the crystal structure of phase II of NH_4N_3 imperative.

In this work, we combine high-pressure XRD and Raman experiments up to 85 GPa with first-principle calculations to determine the structure of AA-II and investigate its stability under high pressure.

II. METHODS

1. Experiments

The NH_4N_3 powder samples were synthesized by a metathetical reaction of NaN_3 and NH_4NO_3 as reported in the literature[21]. The synthesized sample is a colorless and transparent polycrystalline powder. Raman measurements on the synthesized samples confirmed the absence of impurities (Figure S1 in Supporting Information).

The high-pressure measurements were performed in a membrane diamond anvil cell (DAC)[22]. Ruby balls with a diameter of 4 to10 μm were used as pressure sensor[23]. We used diamond anvils with a culet diameter of 200 to 500 μm, depending on the targeted pressure range. For the Raman experiments, type-IIas low fluorescence diamonds were used. T301 steel (for low pressures) or Re (for high pressures) of initial thickness of 200 μm served as gasket material and were preindented to a thickness of 30 to 40 μm. The sample chamber diameter varied from 90 to 200 μm.

For both XRD and Raman experiments, we performed two runs, one without and one with a pressure transmitting medium. In runs without a pressure medium, the sample chamber was

completely filled with AA and the cell rapidly sealed to prevent decomposition known to rapidly occur in air at ambient conditions. In runs with a pressure medium, the sample chamber was loaded with a sample of lateral size 40 to 50 μm. The cell was then rapidly sealed and put in a closed cylinder where argon (in the Raman experiment) or nitrogen (in the XRD experiment) was condensed at liquid nitrogen temperature. The cell was then opened again to fill the sample chamber with liquid argon or liquid nitrogen. The deviatoric stresses measured in argon and nitrogen medium have been found to be of similar magnitude (below 0.1 GPa up to 10 GPa and increasing to ~1.2 GPa at 40 GPa)[24]. As shown hereafter, we did not find significant differences between the results obtained with and without a pressure medium, which likely results from the fact that AA is a soft material with a low bulk modulus.

In the first XRD experiment (no pressure medium), powder XRD patterns were recorded at 300 K in the pressure range 0.9-13.8 GPa using the Mo-Kα radiation of a Rigaku MM007HF rotating anode equipped with an in-house diffractometer and a Rigaku RAXIS-IV detector. The x-ray beam was focused to a diameter of 200 μm at the sample position using x-ray optics. The sample distance, detector tilts and beam center were calibrated with a Si standard. In the second run (with nitrogen pressure medium), we recorded x-ray diffraction patterns from 27.3 to 47 GPa at 300 K at the beamline PSICHÉ of the Soleil Synchrotron Radiation Facility. The x-ray beam had a wavelength of 0.3738 Å and was focused to a spot size of about 15 μm FWHM. Diffracted x-rays were collected by a PILATUS3 X CdTe 2M detector from DECTRIS. The calibration was performed with a CeO_2 powder standard. In this run, pressure was determined from the volume of a small piece of gold powder placed in the sample chamber, using the equation of state of Ref.[25]. The FullProf suite of programs[26] and Vesta[27] were used for Rietveld or Le Bail refinement and visualization of the crystal structures, respectively.

Raman scattering was excited by the 514.5 nm line of an argon laser, collected by a confocal in-house optical set-up and dispersed by a HR460 (Horiba, focal length 460 mm) spectrometer onto a Peltier cooled CCD camera (Andor). The diameter of the laser spot on the sample, focused by 20X Mitutoyo objective, was about 2 μm. Raman spectra were recorded in the range of 70 to 3450 cm-1 using a 1200 lines/mm grating. The covered pressure ranges were 1.8-46 GPa for the sample with argon pressure medium and 9-85 GPa for the sample without pressure medium.

2. Theoretical calculations

The enthalpies and vibrational spectrum of different NH_4N_3 phases were calculated, respectively, by the first-principle plane-wave pseudo-potential density functional theory (DFT) and density functional perturbation theory (DFPT)[28-29], as implemented in the CASTEP code[30]. The ultrasoft pseudopotentials were used with exchange and correlation effects described by the generalized-gradient-approximation (GGA)[31] of Perdew–Burke–Ernzerhof (PBE) for enthalpy calculation, and norm-conserving pseudopotentials for vibrational calculations. The kinetic energy cutoff for structural optimization was set at 898 eV, and Monkhorst-Pack k-point meshes (5×5×2 meshes) were set at 0.07 A^{-1}. The self-consistent energy convergence criterium was set to less than 5.0×10^{-6} eV/atom, and the maximal force, stress and displacement set to be 0.01 eV/Å, 0.02 GPa and 5.0×10^{-4} Å, respectively. The vibration frequencies were calculated after structural optimization, and the "Vibrational Analysis" tool in Material studio software was used for further analysis of the Raman spectra and identification of the vibrational modes.

III. RESULTS AND DISCUSSION

1. High-pressure crystal structure of ammonium azide

In the first XRD experiment, XRD patterns were collected from the pure AA sample (no pressure medium) at 0.9, 3, 7.3 and 13.8 GPa. The XRD patterns at 0.9 GPa and 7.3 GPa are shown in Figure 2. The Bragg reflections in the lower pressure pattern are indexed by the AA-*Pmna* phase as expected, with a small contribution of a second, cubic phase originating from the diffraction of the stainless steel gasket containing the sample. This pattern was refined using the Rietveld method for the AA phase and the Le Bail method for the steel phase, taking for the latter the *Im-3m* structure of pure Fe. Details of the refinement are given in the Supporting Information (Table S2). The refined structural parameters are listed in Table 1 and agree well with the literature[15-17].

The x-ray patterns collected at 3 GPa and above largely differs from the one at 0.9 GPa, confirming the change in the crystal structure of AA previously reported at 2.9 GPa [19-20]. The present pattern at 7.3 GPa, shown in Fig. 2b, is very similar to that reported at 6.6 GPa by Wu et al[16]. For structural refinement, we considered the two structures which have been predicted stable at this pressure, that is, AA-*P2/c*[18] and HNS-2[14]. The simulation of the powder XRD pattern of these two structures clearly showed a good match with the experiment for AA-*P2/c* but not for HNS-2. We thus proceeded with the Rietveld refinement of the XRD pattern using the AA-*P2/c* structural parameters given by our DFT optimization at 6 GPa as initial values. As for the lower pressure, a second phase (*Im-3m*) was included to account for the gasket diffraction. The final refinement result is presented in Figure 2b, showing very good agreement with the experimental data (R_{Bragg}=4.5%). The unit cell and atomic parameters are given in Table 1 (more details in Table S2). Similar results were found at 3 and 13.8 GPa.

We also find very good agreement between the volumes of the *P2/c* phase measured in both XRD experiments (with and without pressure medium) and those determined from our theoretical calculations, as shown in Figure 2. We note that the AA sample embedded in nitrogen was not a good powder (see supplementary figure S2), and Rietveld refinement was thus not possible in this case. Moreover, the diffraction peaks from N_2 merged with some peaks from AA. We thus only extracted the volume of the *P2/c* phase as a function of pressure from this data set. Using the Vinet equation[32] to fit our theoretical P-V data, the ambient pressure volume V_0, bulk modulus B_0 and first-derivative of the bulk modulus B_0' for the *P2/c* phase are 18.8 (9) $Å^3$, 12.8 (4) GPa, and 6.14 (4), respectively. The value of B_0 is in the typical range for hydrogen-bonded molecular solids, and shows that AA-*P2/c* is a soft material.

In order to confirm the XRD results, we compared the experimental Raman spectra of the sample at 6.9 GPa to those of the AA-*P2/c*, AA-*Pmna* and HNS-2 structures computed by DFPT at 6 GPa. As seen in Figure 4, there is a very good match in the number of modes, frequencies and intensities between the experimental spectra and the calculated one for *P2/c* (this will be lengthier discussed in the next section), whereas HNS-2 display a very different Raman spectrum. As shown thereafter, the good agreement also concerns the pressure dependence of the Raman modes.

To supplement the experimental observations, we compared the enthalpies of the different high pressure structures of AA as a function of pressure. At ambient pressure, we find that the total energies per atom of these structures are in the following order: AA-*Pmna* < AA-*P2/c*< TTZ< HNS-1< HNS-2. The relative enthalpies of these structures as a function of pressure are shown in Figure 1(b). Above 4.9 GPa, AA-*P2/c* becomes the lowest energy structure and remains so until 102.6 GPa. Considering that these calculations are performed at 0 K, i.e. thermal effects are not

included, the theoretical transition pressure compares very well with the experimental one at 300 K (2.9 GPa).

The above results thus show that the crystal structure of AA above 2.9 GPa, referred hereafter as AA-II, is the monoclinic *P2/c* structure. As AA-I, this structure is composed of ammonium and azide ions, with two formula units per unit cell. The structures of AA-I (*Pmna*) and AA-II (*P2/c*) are compared in Figure 5. It can be seen that they both are comprised of alternating molecular planes of ammonium and azide ions, held together by hydrogen bonds between the two ionic species. While the ammonium ions are similarly oriented in the two phases, the orientation of the azide ions largely differ. As a matter of fact, AA-I contains two different types of N_3 which are respectively coplanar and perpendicular to the molecular planes, while AA-II only presents one type which is tilted by 39° with respect to the molecular planes. This results in a flatter geometry of the N_3 planes, and thus a more compact structure in the direction perpendicular to the molecular layers. Indeed, while the in-plane distance between ammonium ions increase from 4.33 Å to 5.32 Å, the interlayer distance decreases from 4.22 Å to 3.45 Å between AA-I and AA-II at 6.0 GPa in our calculated structure. The AA-II structure thus achieves a denser packing of the molecular planes while preserving the hydrogen bond network which holds the planes together.

2. Evolution with pressure to 85 GPa.

As said above, our calculations predict that AA-*P2/c* is more stable than all the other predicted structures up to 102 GPa. To check these theoretical results, we performed Raman experiments and compared the pressure evolution of the Raman spectra with that computed for the *P2/c* structure.

The experimental Raman spectra collected from 3.7 to 85 GPa are displayed in Figure 6, while the calculated Raman spectra of AA-*P2/c* from 6.0 to 80 GPa are shown in Figure S3 of the Supporting Information. We found no significant difference between the Raman spectra obtained in experiments with and without pressure medium (a comparison is made in supplementary figure S4), so the displayed spectra in Figure 6 include those collected from the sample embedded in argon up to 46 GPa, and from the one without pressure medium at higher pressures. All the Raman spectra were collected in the range of 70-3450 cm^{-1}, which is displayed in Figure 6 divided into three main regions: low frequency (0-800 cm^{-1}), middle frequency (1100-1900 cm^{-1}) and high frequency (2700-3450 cm^{-1}). The variation with pressure of the frequencies of all the observed and calculated modes are plotted in Figure 7.

The AA-*P2/c* structure has 16 atoms per unit cell resulting in 48 vibrational modes, the symmetry decomposition of the vibrational modes at the center of the Brillouin zone is as follows:

$\Gamma acoustic = Au \oplus 2Bu$

$\Gamma optical = 12Au \oplus 12Bu \oplus 10Ag \oplus 11Bg$

The optical Au and Bu modes are IR active, whereas Ag and Bg are Raman active. The calculated optical modes and their assignment at 6.0 GPa are given in Table S4 of the Supporting Information. The vibrational modes, sorted by increasing frequency, are hereafter referred by their number as reported in Table S4.

The low-frequency region contains 7 lattice vibrational modes with frequencies below 350 cm^{-1} at 5 GPa (modes M4 to M9 and M15). Below 30 GPa, the frequencies of the M6 and M7 vibrations are very close and not resolved in the experimental spectra, but they gradually separate

above 33 GPa, as previously observed in reference [12]. Modes M20 and M22 (556.5 and 614.7 cm^{-1} at 3.7 GPa) arise from torsional motion of NH_4^+. Their predicted Raman intensities are very low which explains why they were not observed in the present and past experiments. Overall, there is a very good correlation between the experimental and theoretical frequency evolution with pressure for the lattice vibrations.

The middle-frequency region contains the N_3 symmetric stretching (M27, and M28) modes, N-H scissoring and wagging (M32-M34) and the N-H bending (M36, M37) modes. Only two modes are observed at the expected positions of M32-M34, which is explained by the close proximity of M32 and M33. Moreover, a Fermi resonance occurs between the N_3 stretching and NH_4 wagging modes, as previously discussed by Medvedev et al.[33], resulting in an intensity conversion and frequency shifts of these modes. This resonance is not accounted for in our calculations at the harmonic level, therefore explaining the differences between experiment and theory.

In the high-frequency region, the spectrum is dominated by the bands corresponding to the four symmetric N-H stretching modes, M44, M45, M47 and M48. M44 and M45 are too close in frequency at all pressures to be resolved and only separated from M47 above 10 GPa in the experiment. However, the broadening of the bands, which becomes significant above 25 GPa, hampers the precise location of the individual modes, which could explain the divergence in pressure between experiment and theory for the M44+M45 modes. The Raman band peaked at 2825 cm^{-1} at 3.7 GPa, not predicted by our calculations, is most likely due to a combination involving N-H bending modes (M36, M37) and N-H scissoring-wagging modes (M32, M33)[33].

As noted in previous works [13, 20], the N-H stretching modes in AA-II first decrease in frequency with pressure up and reach a minimum value of around 15 GPa before increasing again. In our calculations, the same behavior is predicted for modes M47 and M48 of the *P2/c* structure. Since the frequency of the N-H stretching is strongly influenced by hydrogen bonding, the observed behavior was interpreted by an initial strengthening of the H-bonds from 3 to 15 GPa, followed by a weakening of the bonds at higher pressures [20].

The strength of H-bonds is directly related to the bond distance and angle, which we can access by calculation using the DFT optimized structure at each pressure. Figure 8 shows the plots for the two different H-bonds (HB1 and HB2) present in the *P2/c* structure. It can be seen that both bonds exhibit the same evolution as pressure, actually tending to the same length and angle with pressure. Over the whole investigated pressure range, the H-bond lengths H···N monotonically and rapidly decrease from 1.903 Å at 3 GPa to 1.426 Å at 100 GPa, being 1.735 Å at 15 GPa. On the other hand, the bond angles exhibit a non-monotonic behavior, first increasing by about 1° up to 15-20 GPa, and next decreasing by about 2° up to 100 GPa. In general, the closer the bond angle is to 180°, the stronger it is, and it is thus tempting to correlate the observed variation of the N-H stretching frequencies to that of the bond angle; however since the bond length continuously decreases over the same pressure range, it is difficult to conclude whether the H-bond strengthens or not just by looking at these two parameters. A more elaborate analysis of the H-bond energetics is required, which is beyond the scope of the present work.

3. Stability of AA under pressure

The good agreement between the experimental and theoretical Raman spectra seen above shows that the AA-*P2/c* structure remains stable to at least 85 GPa. Using DFT, we investigated

the difference in enthalpy between AA-*P2/c* and AA-*Pmna*, TTZ, HNS-1 and HNS-2 up to 120 GPa. The results are plotted in Figure 1b. They predict a phase transition from AA-*P2/c* to the HNS-1 structure at 102.6 GPa. We recall that the HNS-1 structure contains infinite 1-D zigzag nitrogen chains saturated by hydrogen, in a monoclinic unit cell of $P2_1/m$ space group symmetry, and is thus no more an ammonium azide solid. In addition, we find no pressure range of stability for the TTZ structure. This contrasts with previous theoretical calculations[11-14], which all predicted that AA first transforms to TTZ at pressures ranging from about 40 to 77 GPa. This discrepancy is easily explained in the case of Refs[11-14], as they considered the differences in enthalpy with respect to the *Pmna* structure, while we show here that AA adopts the *P2/c* structure with lower enthalpy than *Pmna* above 3 GPa. The disagreement with Yu et al. cannot be explained in the same way since these authors also considered the difference in enthalpy with respect to the *P2/c* structure, but may come from the different theoretical methods used in the two studies. As a matter of fact, Yu et al. corrected the computed enthalpies obtained with the PBE exchange-correlation function by including van der Waals interactions[18], which was not done in the present work. This correction lowers the enthalpy of TTZ, making it more stable than AA-*P2/c* above 77 GPa. Our experiments show that that *P2/c* is still stable at this pressure, thus indicating that the van-der-Walls correction overstabilize TTZ. Experiments to pressures above 85 GPa are now needed to check the existence of the HNS-1 solid above 1 Mbar.

IV. CONCLUSIONS

We have determined the long-time sought crystal structure of ammonium azide phase II, using high-pressure XRD and Raman experiments coupled to first-principles calculations. Our studies reveal that AA-II structure is monoclinic with space group *P2/c* and can be described as a packing of alternating ammonium and azide layers, held together by hydrogen bonds. The packing is denser

than in AA-I in the direction perpendicular to the layers, due to the reorientation of the azide ions at the transition. The experimental Raman spectra of AA was measured to 85 GPa and correlates very well with the predicted behavior for the vibrational modes of *P2/c* structure computed by DFPT. In addition, all the previous spectroscopic observations made in AA above 3 GPa are well explained by the *P2/c* structure.

Our experiments also demonstrate the absence of phase transition from 3 to 85 GPa, which is consistent with our DFT calculations. The latter predicts the transition to the hydronitrogen solid with 1D zigzag chains of nitrogen saturated by hydrogen at 102.6 GPa, while no pressure range of stability is found for the TTZ solid. This should motivate future investigations in order to extend the pressure range of experimental studies. This work thus reveals that AA is even more stable under pressure that previously thought, making the compression of pure AA a non-practical way to obtain hydronitrogen solids. However, a recent theoretical work predicted an easier route by reacting AA with molecular nitrogen at pressures in the range of 10 GPa[34], which should be explored in future studies.

ASSOCIATED CONTENT

Supporting Information.

Figure S1. Raman spectra of the synthesized NH_4N_3 powder sample at ambient conditions.

Figure S2. X-ray diffraction image of the AA sample embedded in nitrogen pressure medium at 28.2 GPa and 300 K

Figure S3. Calculated Raman spectra of AA-*P2/c* at different pressures.

Figure S4. Comparison of the experimental Raman frequencies of AA as a function of pressure for the sample compressed in argon pressure medium and for the one with no pressure medium.

Table S1. Comparison of our calculation results for the DFT optimized structures at ambient pressure with previous theoretical calculations.

Table S2. Details of the Rietveld refinement of the XRD patterns at different pressures.

Table S3. Lattice parameters and volume of the *P2/c* phase as a function of pressure obtained in present theoretical calculations.

Table S4. Calculated optical modes of AA-*P2/c* at 6.0 GPa.

AUTHOR INFORMATION

Corresponding Author

*E-mail: cc060109@qq.com; frederic.datchi@sorbonne-universite.fr

Notes

The authors declare no competing financial interests.

ACKNOWLEDGMENT

We thank Keevin Beneut for assistance in using the spectroscopic facilities of the IMPMC, and Benoit Baptiste and Ludovic Delbes for assistance in using the diffraction facilities of the IMPMC. We acknowledge the SOLEIL synchrotron for provision of beamtime at beamline PSICHÉ under proposal 20190912. This work was supported by the Chinese Scholarship Council through the allocation of a scholarship to Guozhao ZHANG, the National Natural Science Foundation of China (Grant Nos. 11674404, 11874174, and 11774128), the National Science Foundation of Shandong Province (ZR2018JL003) and the French Agence Nationale de la Recherche under grant ANR-15-CE30-0008-01 (SUPER-ICES)

REFERENCES

(1) Qian, G.-R.; Niu, H.; Hu, C.-H.; Oganov, A. R.; Zeng, Q.; Zhou, H.-Y., Diverse Chemistry of Stable Hydronitrogens, and Implications for Planetary and Materials Sciences. *Sci. Rep.* **2016**, *6*, 25947.

(2) Wang, H.; Eremets, M. I.; Troyan, I.; Liu, H.; Ma, Y.; Vereecken, L., Nitrogen Backbone Oligomers. *Sci. Rep.* **2015**, *5*, 13239.

(3) Goncharov, A. F.; Holtgrewe, N.; Qian, G.; Hu, C.; Oganov, A. R.; Somayazulu, M.; Stavrou, E.; Pickard, C. J.; Berlie, A.; Yen, F., Backbone N_xH Compounds at High Pressures. *J. Chem. Phys.* **2015**, *142*, 214308.

(4) Spaulding, D. K.; Weck, G.; Loubeyre, P.; Datchi, F.; Dumas, P.; Hanfland, M., Pressure-Induced Chemistry in a Nitrogen-Hydrogen Host-Guest Structure. *Nat. Commun.* **2014**, *5*, 5739.

(5) Eremets, M. I.; Gavriliuk, A. G.; Trojan, I. A.; Dzivenko, D. A.; Boehler, R., Single-Bonded Cubic Form of Nitrogen. *Nat. Mater.* **2004**, *3*, 558.

(6) Steele, B. A.; Stavrou, E.; Crowhurst, J. C.; Zaug, J. M.; Prakapenka, V. B.; Oleynik, I. I., High-Pressure Synthesis of a Pentazolate Salt. *Chem. Mater.* **2016**, *29*, 735-741.

(7) Sun, C.; Zhang, C.; Jiang, C.; Yang, C.; Du, Y.; Zhao, Y.; Hu, B.; Zheng, Z.; Christe, K. O., Synthesis of AgN_5 and Its Extended 3D Energetic Framework. *Nat. Commun.* **2018**, *9*, 1269.

(8) Yin, K.; Wang, Y.; Liu, H.; Peng, F.; Zhang, L., N_2H: a Novel Polymeric Hydronitrogen as a High Energy Density Material. *J. Mater. Chem. A* **2015**, *3*, 4188-4194.

(9) Laniel, D.; Weck, G.; Gaiffe, G.; Garbarino, G.; Loubeyre, P., High-Pressure Synthesized Lithium Pentazolate Compound Metastable under Ambient Conditions. *J. Phys. Chem. Lett.* **2018**, *9*, 1600-1604.

(10) Batyrev, I. G., Modeling of Extended N-H Solids at High Pressures. *J. Phys. Chem. A* **2017**, *121*, 638-647.

(11) Hu, A.; Zhang, F., A Hydronitrogen Solid: High Pressure Ab Initio Evolutionary Structure Searches. *J. Phys. Condens. Matter* **2010**, *23*, 022203.
(12) Crowhurst, J. C.; Zaug, J. M.; Radousky, H. B.; Steele, B. A.; Landerville, A. C.; Oleynik, I. I., Ammonium Azide under High Pressure: a Combined Theoretical and Experimental Study. *J. Phys. Chem. A* **2014**, *118*, 8695-700.
(13) Yedukondalu, N.; Vaitheeswaran, G.; Anees, P.; Valsakumar, M. C., Phase Stability and Lattice Dynamics of Ammonium Azide under Hydrostatic Compression. *Phys. Chem. Chem. Phys.* **2015**, *17*, 29210-29225.
(14) Liu, Q.-J.; Zhang, N.-C.; Sun, Y.-Y.; Zhang, M.-J.; Liu, F.-S.; Liu, Z.-T., Density-Functional Theory Study of the Pressure-Induced Phase Transition in Hydronitrogen Compound N_4H_4. *Phys. Lett. A* **2014**, *378*, 1333-1335.
(15) Prince, E.; Choi, C. S., Ammonium Azide. *Acta Cryst. B* **1978**, *34*, 2606-2608.
(16) Wu, X.; Cui, H.; Zhang, J.; Cong, R.; Zhu, H.; Cui, Q., High Pressure Synchrotron X-Ray Diffraction and Raman Scattering Studies of Ammonium Azide. *Appl. Phys. Lett.* **2013**, *102*, 121902.
(17) Salim de Amorim, H.; do Amaral Jr, M. R.; Pattison, P.; Pereira Ludka, I.; Mendes, J. C., Ammonium Azide: A Commented Example of an Ab Initio Structure (Re-)Determination From X-Ray Powder Diffraction. *Rev. Soc. Quim. Mex.* **2002**, *46*, 313-319.
(18) Yu, H.; Duan, D.; Tian, F.; Liu, H.; Li, D.; Huang, X.; Liu, Y.; Liu, B.; Cui, T., Polymerization of Nitrogen in Ammonium Azide at High Pressures. *J. Phys. Chem. C* **2015**, *119*, 25268-25272.
(19) Medvedev, S. A.; Eremets, M. I.; Evers, J.; Klapötke, T. M.; Palasyuk, T.; Trojan, I. A., Pressure Induced Polymorphism in Ammonium Azide (NH_4N_3). *Chem. Phys.* **2011**, *386*, 41-44.
(20) Wu, X.; Ma, F.; Ma, C.; Cui, H.; Liu, Z.; Zhu, H.; Wang, X.; Cui, Q., Pressure-Driven Variations of Hydrogen Bonding Energy in Ammonium Azide (NH_4N_3): IR Absorption and Raman Scattering Studies. *J. Chem. Phys.* **2014**, *141*, 024703.
(21) Frierson, W. J.; Browne, A. W., Preparation of Ammonium Trinitride from Dry Mixtures of Sodium Trinitride and an Ammonium Salt. *J. Am. Chem. Soc.* **1934**, *56*, 2384-2384.
(22) Letoullec, R.; Pinceaux, J. P.; Loubeyre, P., The Membrane Diamond Anvil Cell: a New Device for Generating Continuous Pressure and Temperature Variations. *High Press. Res.* **1988**, *1*, 77-90.
(23) Dewaele, A.; Torrent, M.; Loubeyre, P.; Mezouar, M., Compression Curves of Transition Metals in the Mbar Range: Experiments and Projector Augmented-Wave Calculations. *Phys. Rev. B* **2008**, *78*, 104102.
(24) Klotz, S.; Chervin, J.; Munsch, P.; Le Marchand, G., Hydrostatic Limits of 11 Pressure Transmitting Media. *J. PHYS. D: APPL. PHYS.* **2009**, *42*, 075413.
(25) Fei, Y.; Ricolleau, A.; Frank, M.; Mibe, K.; Shen, G.; Prakapenka, V., Toward an Internally Consistent Pressure Scale. *PNAS* **2007**, *104*, 9182-9186.
(26) Rodríguez-Carvajal, J., Recent Advances in Magnetic Structure Determination by Neutron Powder Diffraction. *Physica B* **1993**, *192*, 55-69.
(27) Momma, K.; Izumi, F., VESTA 3 for Three-Dimensional Visualization of Crystal, Volumetric and Morphology Data. *J. Appl. Crystallogr* **2011**, *44*, 1272-1276.
(28) Baroni, S.; De Gironcoli, S.; Dal Corso, A.; Giannozzi, P., Phonons and Related Crystal Properties from Density-Functional Perturbation Theory. *Rev. Mod. Phys.* **2001**, *73*, 515.

(29) Refson, K.; Tulip, P. R.; Clark, S. J., Variational Density-Functional Perturbation Theory for Dielectrics and Lattice Dynamics. *Phys. Rev. B* **2006**, *73*, 155114.
(30) Segall, M. D.; Lindan, P. J. D.; Probert, M. J.; Pickard, C. J.; Hasnip, P. J.; Clark, S. J.; Payne, M. C., First-Principles Simulation: Ideas, Illustrations and the CASTEP Code. *J. Phys. Condens. Matter* **2002**, *14*, 2717.
(31) Perdew, J. P.; Burke, K.; Ernzerhof, M., Generalized Gradient Approximation Made Simple. *Phys. Rev. Lett.* **1996**, *77*, 3865.
(32) Vinet, P.; Ferrante, J.; Smith, J.; Rose, J., a Universal Equation of State for Solids. *J. Phys. C: Solid State Phys.* **1986**, *19*, L467.
(33) Medvedev, S. A.; Palasyuk, T.; Trojan, I. A.; Naumov, P. G.; Evers, J.; Klapötke, T. M.; Eremets, M. I., Pressure-Tuned Vibrational Resonance Coupling of Intramolecular Fundamentals in Ammonium Azide (NH_4N_3). *Vib. Spectrosc.* **2012**, *58*, 188-192.
(34) Steele, B. A.; Oleynik, I. I., Pentazole and Ammonium Pentazolate: Crystalline Hydro-Nitrogens at High Pressure. *J. Phys. Chem. A* **2017**, *121*, 1808-1813.

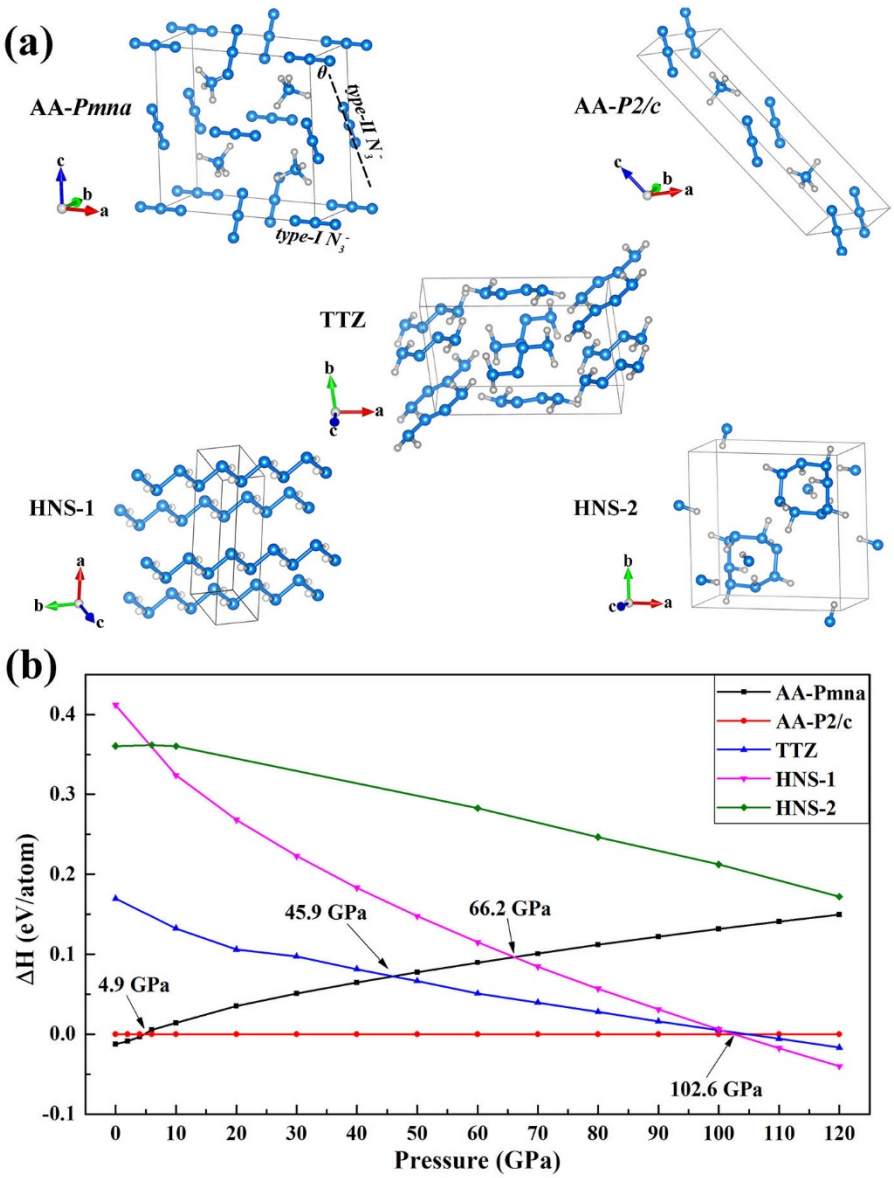

Figure 1. (a) Crystal structures of N_4H_4 compounds; (b) Relative enthalpies of different N_4H_4 structures with respect to the AA-*P2/c* structure (AA-II).

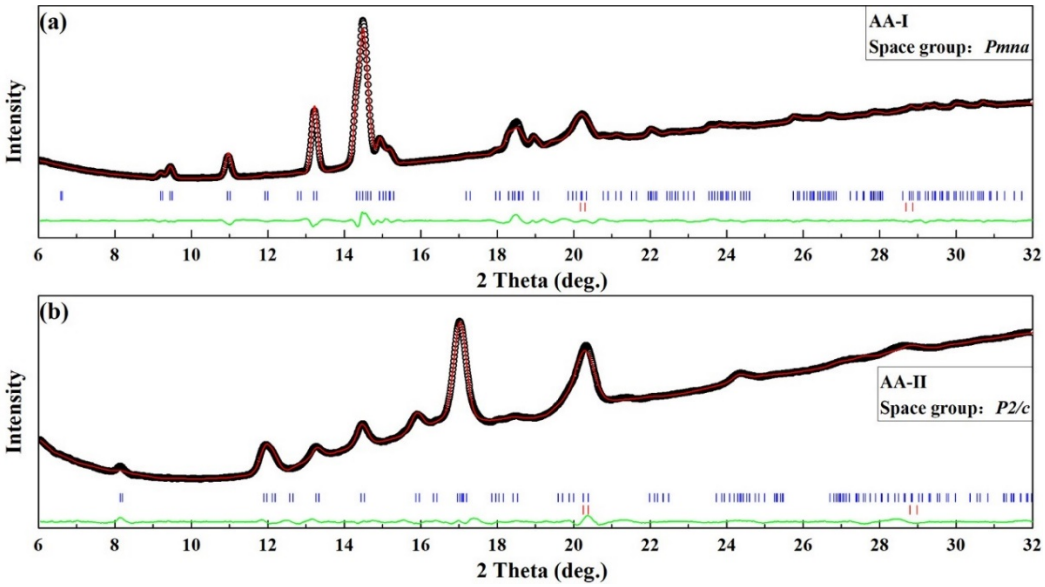

Figure 2. Rietveld refinement of the NH_4N_3 powder x-ray diffraction patterns at (a) 0.9 GPa and (b) 7.3GPa. For both panels, the open circles are the experimental data, the red line is the calculated pattern, blue and red vertical tickmarks refer to Bragg reflections from the sample and the gasket, respectively, and the green line is the difference (observed-calculated) pattern.

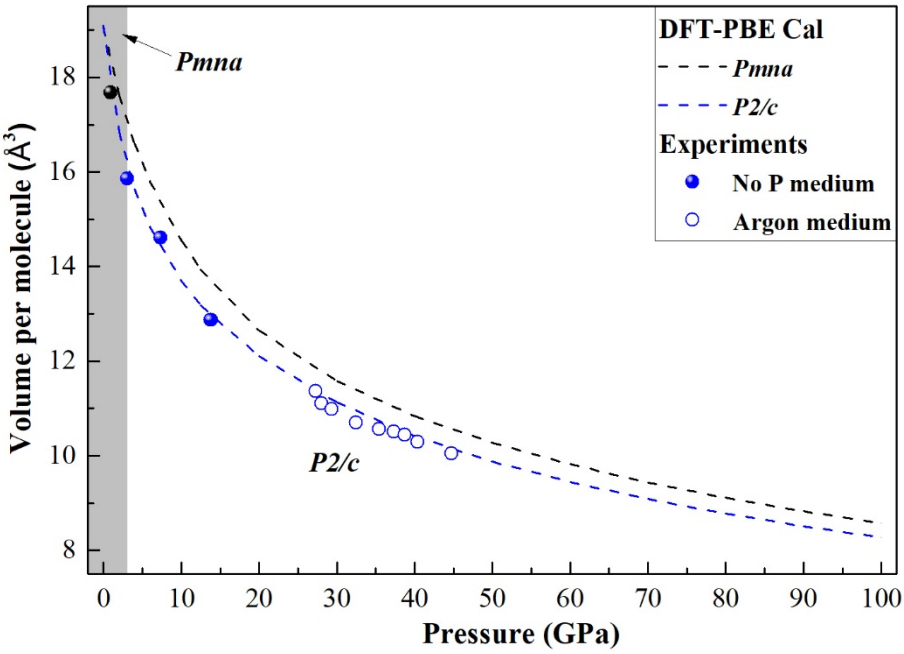

Figure 3. Equation of state of ammonium azide. The black and blue dashed lines are the respective fits to the theoretical V-P datasets using the Vinet equation for AA-*Pmna* and AA-*P2/c*. The solid and open circles represent the data from the sample without and with nitrogen pressure medium, respectively. Error bars are within the symbol size.

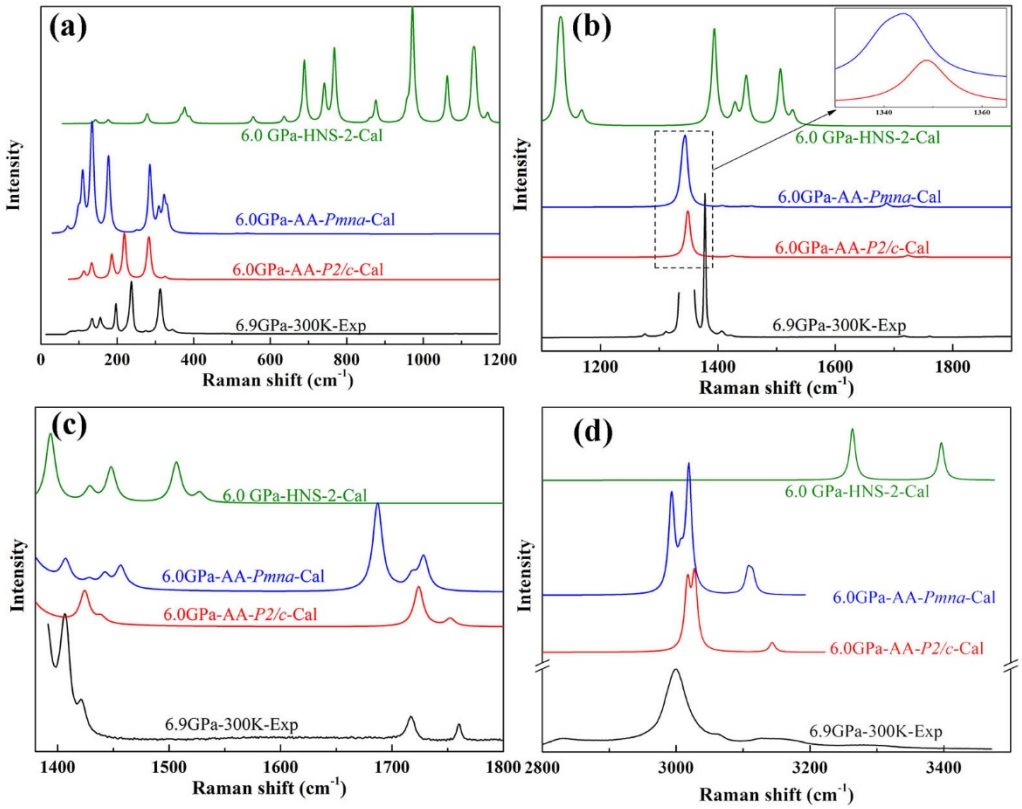

Figure 4. Experimental Raman spectra of AA at 6.9 GPa (labeled "Exp") compared to the calculated ones at 6 GPa using DFPT for the AA-*P2/c*, AA-*Pmna* and HNS-2 structures (labeled "Cal"). The spectra are presented in the four separate panels a-d to independently adjust the intensity scale of different frequency ranges. Note that the strong peak at 1330 cm^{-1} in the experimental spectra of panel b come from the diamond anvils.

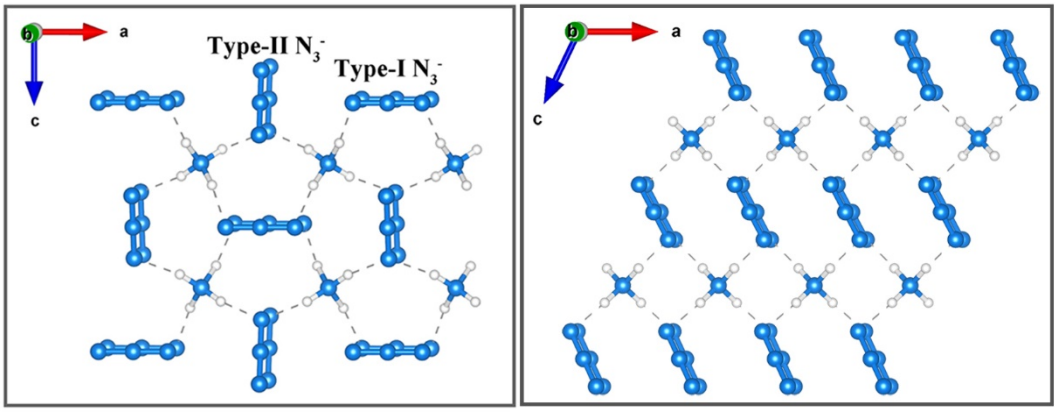

Figure 5. Comparison between (left) the AA-I (*Pmna*) and (right) the AA-II (*P2/c*) structures. The viewing direction is chosen to visualize the alternating molecular layers of ammonium and azide ions. Broken lines represent the N-H···N hydrogen bonds between ammonium and azide ions.

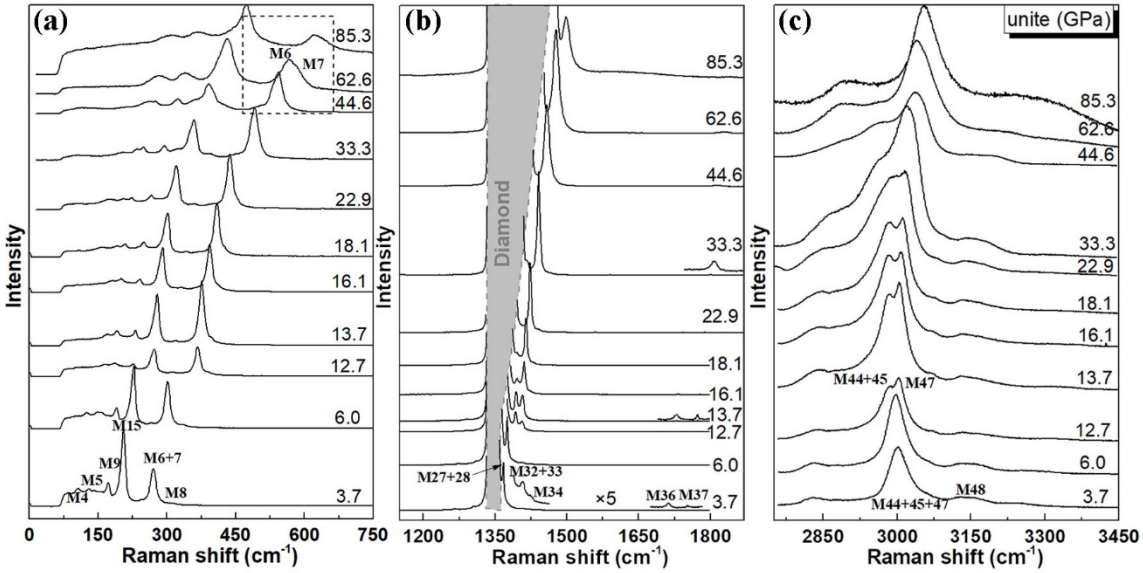

Figure 6. Pressure evolution of Raman spectra of NH_4N_3 up to 85 GPa at ambient temperature. Numbers preceded by M refers to the numbering of Raman modes given in the Supporting Information Table S4. The pressure is indicated in GPa.

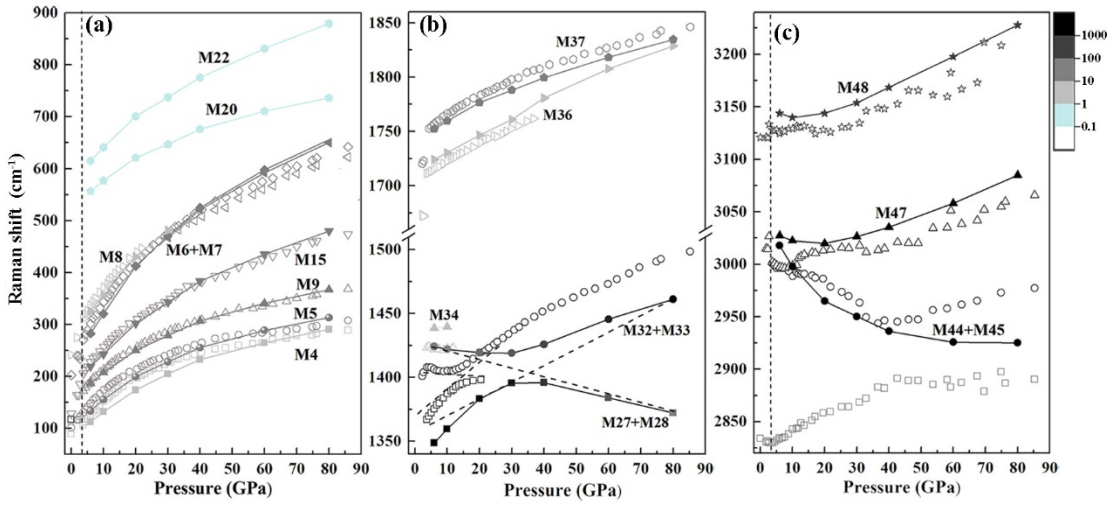

Figure 7. Pressure evolution of the frequencies of the Raman vibrational modes of NH_4N_3 up to 85 GPa. The open symbols are experimental Raman data, and the solid symbols are the calculated Raman frequencies of AA-*P2/c*. The vertical dashed line at 3.0 GPa delineates the transition pressure from phase I to phase II. Color scale indicates the intensity of the Raman mode, numbers preceded by M refers to the numbering of Raman modes given in the supplementary Table S4.

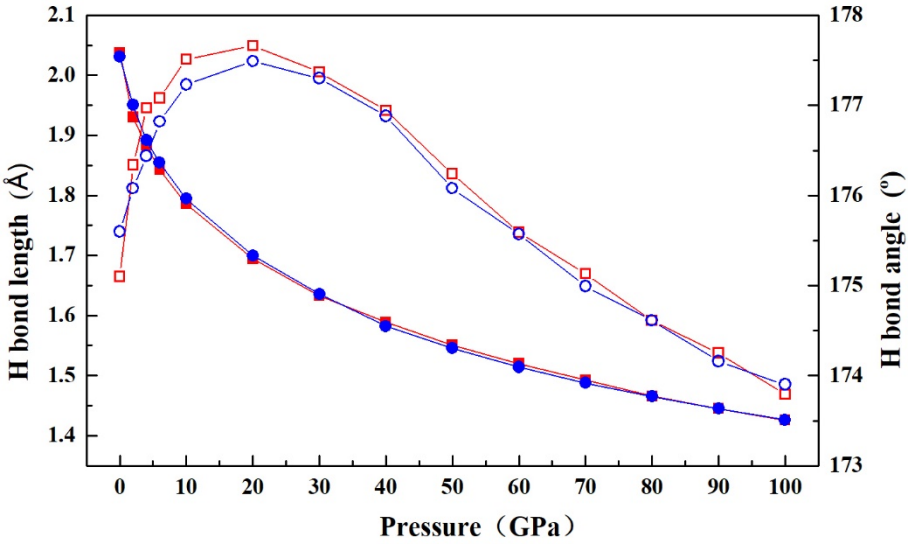

Figure 8. Lengths (solid symbols) and angles (open symbols) of the two H-bonds (red squares: N3-H1···N2, blue circles: N3-H2···N2) in the AA-*P2/c* structure as a function of pressure, as obtained by present DFT calculations.

Table 1. Results of the Rietveld refinements of the x-ray powder patterns at 0.9 GPa (*Pmna* phase, top panel) and 7.3 GPa (*P2/c* phase, bottom panel) at 295 K. The final R_{Bragg} agreement factor is 5.1% at 0.9 GPa and 4.4% at 7. 3 GPa.

Phase	Atoms	Wyck	x	y	z
Pmna	N (1) (middle) of type I N_3^-	2a	0	0	0
	N (2) (middle) of type II N_3^-	2b	0.5	0	0
	N (3) (terminal) of type I N_3^-	4e	0.13553	0	0
a=8.843(1) Å	N (4) (terminal) of type II N_3^-	4h	0.5	0.12827	0.12746
b=3.713(1) Å	N (5) of NH_4^+	4g	0.25	0.52206	0.25
c=8.611(1) Å	H (1)	8i	0.30107	0.72845	0.33472
	H (2)	8i	0.33030	0.41095	0.19583
P2/c					
	N (1) (middle) of N_3^-	2d	-0.5	0	0
	N (2) (terminal) of N_3^-	4g	-0.21124	-0.8267	0.08002
a=3.420(1) Å	N (3) of NH_4^+	2f	0.5	-0.38508	0.25
b=3.420(1) Å	H (1)	4g	0.41085	-0.54440	0.30898
c=11.118(8) Å	H (2)	4g	-0.236	-0.1909	0.30886

TOC Graphic